Advances in Science and Technology Research Journal

Advances in Science and Technology Research Journal 2023, 17(6), 164–170
https://doi.org/10.12913/22998624/174516
ISSN 2299-8624, License CC-BY 4.0

Received: 2023.09.15
Accepted: 2023.10.25
Published: 2023.11.21

Simulation of SESAME's Synchrotron Storage Ring for the Pressure Predictions in Vacuum System

Firas Makahleh[1], Hani Attar[2], Ahmad Manasrah[1], Anas Nassar[1], Ayman Amer[2], Sameh Alsaqoor[3,4], Gabriel Borowski[5], Ali Alahmer[3,6]

[1] Mechanical Engineering, Mechanical Engineering Dept., Al-Zaytoonah University of Jordan, P.O. Box 130, Amman, 11733, Jordan
[2] Energy Engineering, Department, Faculty of Engineering Technology, Zarqa University, Zarqa, Jordan
[3] Department of Mechanical Engineering, Faculty of Engineering, Tafila Technical University, Tafila, Jordan
[4] Renewable Energy Technology, Applied Science Private University, Amman, Jordan
[5] Faculty of Environmental Engineering, Lublin University of Technology, Nadbystrzycka 40B, 20-618 Lublin, Poland
[6] Department of Mechanical Engineering, Tuskegee University, Tuskegee, AL 36088, United States of America
* Corresponding author's e-mail: sameh@ttu.edu.jo

ABSTRACT

Many particle accelerators rely on maintaining low pressures to ensure efficient operation, minimize beam losses, and reduce radiation background. To ensure a beam lifetime of 1–20 hours for the Synchrotron-light for Experimental Science and Applications in the Middle East (SESAME) vacuum system, an ideal average dynamic pressure of 1×10^{-9} mbar was targeted. This pressure was intended to be maintained while running the accelerator at a current of 400 mA after a cumulative dose of 100 Ah. In this study, a MATLAB code was employed to develop a series of one-dimensional equations that simulate the behavior of the vacuum system within the SESAME storage ring. The proposed model was then compared with the results generated by the VACCALC software and the Particle Monte Carlo (TPMC) MOLFLOW code, establishing a comprehensive assessment framework. The collected data from the model was subsequently compared with the recorded static and dynamic pressure measurements obtained during more than 1000 Ah of beam conditioning at 2.5 GeV. In results, the projected and actual values of dynamic pressures exhibited a satisfactory degree of agreement across the investigated range of beam conditioning doses, with a consistency factor exceeding 2 after a 100 Ah dose.

Keywords: gas flow modelling, photon stimulated desorption, synchrotron light source storage ring, MATLAB.

INTRODUCTION

The Synchrotron-light for Experimental Science and Applications in the Middle East (SESAME) is a cutting-edge third-generation synchrotron light source strategically located near Amman, Jordan. Since its commencement in 2018 [1–3], SESAME has been powered by a storage ring housing sixteen dipole arc chambers, thoughtfully partitioned into eight short and eight long straight chambers. The overall vacuum layout of these sixteen storage ring chambers is illustrated in Figure 1. Meanwhile, Figure 2 provides a comprehensive depiction of the dipole chamber configuration, meticulously delineating the strategic placement of vacuum pumps, dipole magnets, straight sections, and sextupoles.

The storage ring of the synchrotron comprises sixteen individual cells, each encompassing both a dipole arc and a straight chamber (either long or short) that is sealed by a UHV RF shielded gate valve. These vacuum cells can be categorized into two distinct types [4]. The first type features an arc dipole chamber along with long straight

sections, spanning a combined length of 9.35 meters. Conversely, the second type consists of a short straight section, with a collective length of 7.3 meters. The cumulative length of all the vacuum cells aggregates to 133.2 meters. Close to the absorbers, diode sputter ion pumps (SIPs) have been incorporated, boasting a combined nominal pumping speed of 20400 L/s. Additionally, near the absorbers characterized by elevated SR (synchrotron radiation) absorption and subsequently increased outgassing, non-evaporable getter (NEG) pumps have been strategically positioned. It is noteworthy that the simulation does not encompass the impact of the NEG pumps.

The remaining three straight sections fulfill distinct functions: they serve as areas for kickers, injections, and radio frequency (RF) operations. As per the design criteria, following a beam conditioning of 100 Ah, the storage ring is supposed to achieve an ultimate pressure of 10^{-9} mbar (CO equivalent) or even lower, while accommodating a stored beam of 400 mA.

The lifetime of the Gas Bremsstrahlung radiation emission of the stored beam critically hinges on the ultimate operating pressure. This concept is underpinned by the discussion of photon-stimulated desorption yield, elucidated for various vacuum vessel configurations, including factory-baked stainless steel, copper-plated vessels, fired vessels, glow-discharged vessels, and unbaked vessels. These discussions serve as guiding principles for numerous contemporary synchrotrons [5,6]. In the scope of this simulation, the photon-stimulated data obtained from in-situ baked vessel scenarios will be employed both within the simulation and incorporated into the vessel construction and subsequent installation processes.

Synchrotron light/radiation sources have been considered to be one of the most powerful testing tools for scientific exploration [7]. These tools have played a vital role in driving numerous breakthroughs across a wide range of disciplines, encompassing physics, chemistry, materials science, and various other fields. The operational foundation of synchrotrons fundamentally involves propelling high-energy electrons into evacuated chambers, expertly controlled by sophisticated arrangements of magnetic systems [8].

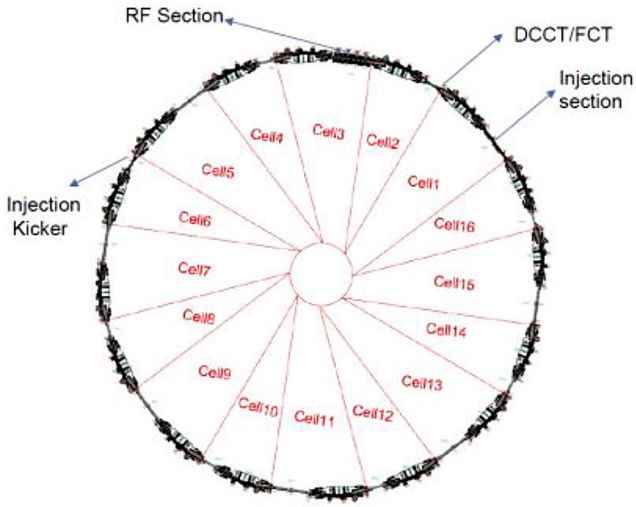

Ion pumps	105 Pumps
Dipole chamber	2 X 300L/S
	2 X 150L/S
Long Straight	3 X 150L/S
Short straight	2 X150L/S
RF Section	4 x 150L/S
NEG pumps	**16**
IMG	**27**
Dipole chamber	16
Long straight	7
RF section	4
RF Valves	**16**
RF Bellows	**34**

Figure 1. Vacuum layout of SESAME storage ring

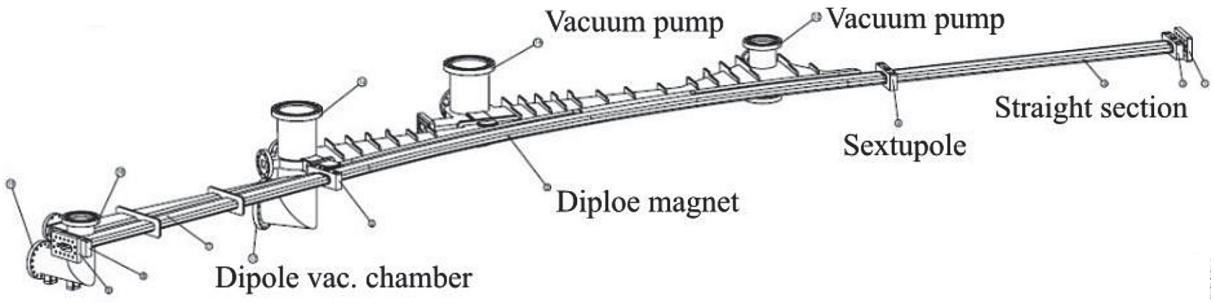

Figure 2. Construction of long straight chambers

Subsequently, these electrons generate streams of radiation and/or light. In the context of third-generation synchrotron light sources such as SESAME, these light beams are captured and confined within vacuum-sealed chambers known as storage rings. As a standard feature, third-generation synchrotrons generate X-ray beamlines, which are employed for the examination of diverse materials and samples. Illustratively, a preceding investigation employed a synchrotron light source to conduct time-elapsed micro-computed tomography (CT) imaging of neck fractures [9]. The study revealed significant potential in the exploration of micromechanics within neck bones, enabling researchers to generate highly detailed imaging of the bone microstructure. An additional illustration of leveraging this tool involves the examination of photovoltaic modules covered with polycarbonate (PC) [10]. In this case, the study explored the potential for fractures at interface points between PC and other materials, employing X-ray beamlines. A similar scenario is demonstrated in [11], where the stability of organic-inorganic metal halide perovskite photovoltaic materials was evaluated through synchrotron X-ray diffraction for optical stability. These assessments underscore the significant advantages of reconsidering flawed designs at the microstructural level. Furthermore, synchrotron light sources have played a pivotal role in advancing medical applications, contributing significantly to various developments in the field. For instance, X-ray beamline screenings have been harnessed in structure-guided drug research, aiding in the identification of fragment hits at the microstructural level [12]. Other studies have employed synchrotron infrared atomic force microscopy to explore biological materials at the subcellular level [13]. Additionally, synchrotron microspectroscopy has been applied to monitor the release of anticancer drug molecules from their composites [14], thereby aiding in the modulation of drug release rates. These finding offer researchers enhanced insights into various aspects of their studies, including the tracking of DNA and genes responsible for drug delivery mechanisms [15].

The development of the SESAME vacuum system proceeded through various phases, aligned with available resources and design development prerequisites:

- Initial project phase: Commencing with the project's inception and the creation of the white book, MOLFLOW was employed [16].
- Elaborate design and manufacturing stage: Advancing from detailed design to manufacturing, the one-dimensional gas dynamic equilibrium of the vacuum vessel was analyzed using MATLAB and VACCALC [17–19].
- Parameter identification phase: A MOLFLOW model was generated to identify essential parameters for the vacuum system [20,21].

The goal of this study was comparison of measurement and simulation results of pressure within accelerator vacuum systems using prediction models from MATLAB, VACCALC, and MOLFLOW software.

METHODOLOGY OF MODELING AND SIMULATION

The initial phase of model generation involves identifying relevant drawings and desorption rates using surface elements in proximity to pump locations. Once pumping characteristics are established, the vacuum system model is constructed through probabilistic methods. These encompass numerical simulations of extensive random molecular motion, involving processes such as ensemble generation, transmission probability calculation, molecular interactions, and their interplay with solid surfaces. To achieve a heightened level of accuracy, a 3D Direct Simulation Monte-Carlo (DSMC) code is employed. This approach effectively captures the intricacies of complex geometrical configurations within vacuum vessels, accounting for obstacles like absorbers and contributing to a more precise model. Conversely, the creation of the DSMC model, which permits adjustments during design optimization, is a time-consuming process demanding specialized personnel, a resource that is seldom readily accessible. The Monte-Carlo method relies on a set of assumptions, including a steady gas flow and adherence to the Maxwell–Boltzmann distribution of molecular velocities under molecular conditions. The calculation procedure initiates by randomly generating the spatial position of a molecule at the entrance orifice of a duct. Subsequently, random cosine directions and velocity vectors are assigned, and this sequence persists until the molecule traverses the duct opening, completing its motion trajectory. This process progression then proceeds with the handling of the next molecule, encompassing the generation

of its spatial coordinates at the duct orifice along with cosine directions, and so forth. The calculation process is deemed finalized once a satisfactory number of molecular histories have been computed, facilitating the accurate determination of probability [22]. An alternative approach involves employing a deterministic method through the solution of kinetic equations. In this study, a one-dimensional (1D) model is employed, based on a balanced equation of gas dynamics within a vacuum vessel, to compute the conductance of individual segments within the vacuum chamber [23]. To assess the pressure values within a unit cell, a code of MATLAB program was developed to solve a linear system of balanced equations pertaining to three consecutive interconnected elements. The unit cell comprises 152 elements, each approximately 11 cm in length, except for elements hosting pumps, which extend to 20 cm. Overall, the total length of the unit cell is approximately 16.3 m.

The governing continuity equations:

$$C_i \cdot (P_{i-1} - P_i) + C_{i+1} \cdot (P_{i+1} - P_i) + Q_i = S_i \cdot P_i \quad (1)$$

$$(i = 1, 2, ..., n = 152)$$

According to the following periodic boundary condition:

$$P_1 = P_{152}$$

where: P_{i-1}, P_i, P_{i+1} – represent unknown pressure of the elements i–1, i and i+1, respectively;
C_i and C_{i+1} – denote the conductance value i and i –1 and between element i and i+1, respectively.

These values are determined by evaluating for CO molecules using the MOLFLOW method; S_i signifies the pumping speed of element i; and Q_i stands for the total gas load of element i.

The gas load, Q_i, is computed as the summation of two distinct terms:

$$Q_i = Q_{pd} + Q_{th} \quad (2)$$

where: Q_{pd} – represents the stimulated photon desorption for the copper absorber;
Q_{th} – indicates the gas load attributed to thermal desorption within the stainless-steel chamber.

In practical units:

$$Q_{pd} = 5.6 \times 10^{-21} \text{ [mbar·L·s}^{-1}\text{]}$$

$$Q_{pd} = 5.6 \times 10^{-21} \times \eta \times N\gamma \times Dq_i \text{ [mbar·L·s}^{-1}\text{]} \quad (3)$$

where: $\eta = 10^{-6}$ molecules/photon represents the yield for OFHC copper subsequent to a dose of 100 Ah;
Dq_i – signifies the angle intercepted by the absorber from the synchrotron radiation fan,
$N\gamma$ – stands for the total number of photons per second per degree, computed using the following approximate formula:

$$N\gamma = 8.08 \times 10^{20} \times E \times I / 360 = 2.25 \times 10^{18} \quad (4)$$
[photons/(degree·s)]

where: E – energy in giga-electronvolt [GeV],
I – current [A].

The gas load, Q_{th}, at a temperature of 20 °C, is finally obtained by multiplying the surface of each element by a typical coefficient of 10^{-11} mbar·L·s^{-1}·cm^{-2}, attainable through effective cleaning and pre-backing processes.

Similarly, analogous to the MATLAB pressure profile calculation, the VACCALC program, designed to determine beam pipe pressure profiles and developed by Michael Sullivan, utilizes the finite difference technique to evaluate pressure distributions. This process entails leveraging insights into outgassing, pumping speed, and conductance for each discrete segment constituting complex vacuum chambers.

The materials composed the vacuum chambers of the accelerators, such as copper and stainless steel, desorb gas into the vacuum system. This process, known as thermal desorption, quantifies the static pressure within the storage ring when no beam is present. The desorption rate assumption draws from historical data across numerous Synchrotron Radiation Sources such as Daresbury, SLS, and SOLEIL. This data includes the information from in-situ baked vacuum vessels that have been nitrogen-vented and subsequently re-pumped.

For the simulation, an outgassing rate of approximately 10^{-11} mbar·L·s^{-1}·cm^{-2} is employed for CO equivalence. Conductance calculations are derived using MOLFLOW software and then integrated into both the MATLAB program and VACCALC. In the MATLAB program, periodic boundary conditions for pressure are iteratively applied for each sector, while these conditions are inherently built into the VACCALC framework. Note that the simulation link was applied as in the references [24-26].

RESULTS

The MATLAB results depicted in Figure 3 closely resemble those predicted by VACCALC, as indicated in Table 1, with a deviation of less than 2% following a dose of 100 Ah. This concurrence is expected, since both methods utilize one-dimensional finite difference techniques; the primary distinction lies in the imposition of periodic boundary conditions within MATLAB. The average pressure computed using MATLAB is 1.26×10^{-9} mbar, in comparison to 1.29×10^{-9} mbar achieved through VACCALC simulation and 1.4×10^{-9} mbar using MOLFLOW.

Table 1 provides a summary of the comparison between the measured data from the SESAME storage ring and the results obtained from various models. This comparison is conducted at dose rates of 0.01, 100, 500, and 1000 Ah. The agreement between the measured pressure and the model results falls within a factor of 2 at 100 Ah, while notably improved outcomes (lower pressure) are observed in the measured data of the MOLFLOW model, achieving results within a factor of 4. Notably, the measured pressure data for the storage ring without the presence of a beam reaches as low as 1.5×10^{-11} mbar. In Figure 4, a comparison is presented between the linear trend

Table 1. Comparison of models versus measurements results

Dose (Ah)	Current (mA)	Models pressure (mbar)			Measurements pressure (mbar)	
		MATLAB	VACCALC	MOLFLOW	With Beam	WO Beam
0.01	10	–	–	$1.26\text{x}10^{-7}$	$2\text{x}10^{-8}$	$3\text{x}10^{-10}$
100	100	$1.26\text{x}10^{-9}$ (at 400 mA)	$1.29\text{x}10^{-9}$ (at 400 mA)	$1.4\text{x}10^{-9}$	$3\text{x}10^{-9}$	$1\text{x}10^{-10}$
500	300	–	–	$1.05\text{x}10^{-9}$	$5\text{x}10^{-10}$	$5\text{x}10^{-11}$
1000	400	–	–	$8.75\text{x}10^{-10}$	$2\text{x}10^{-10}$	$1.5\text{x}10^{-11}$

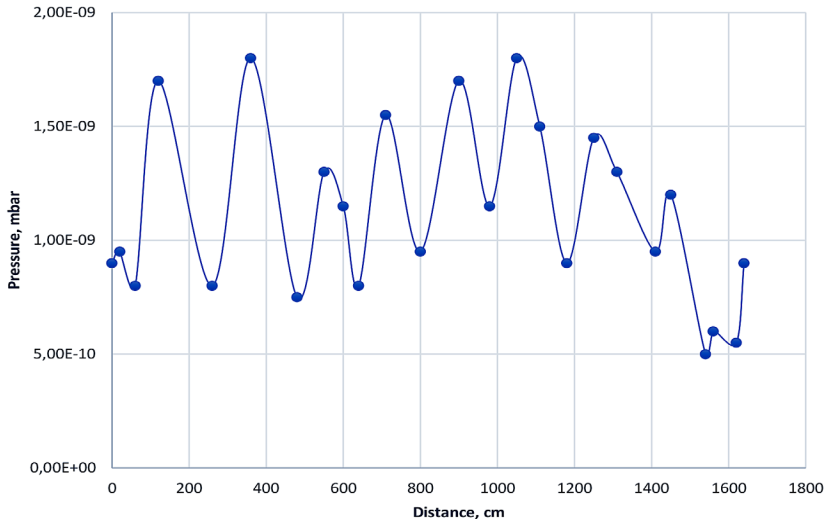

Figure 3. MATLAB simulation results with pressure at 100 Ah

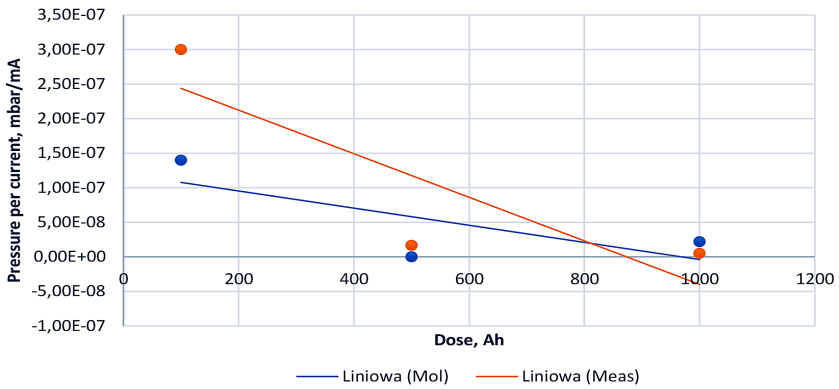

Figure 4. Comparison of pressure versus accumulated dose for storage ring: red line – linear trend of the measured pressure; blue line – linear trend of the model results

of the measured pressure and the linear trend of the model results. Until a dose of 800 Ah, the measurement results exceed the model outcomes, following which the measured value begins to dip below the MOLFLOW simulation results. These measured pressure data contribute to extending the beam lifetime to 24 hours.

CONCLUSIONS

The results demonstrated good agreement between the pressure predictions obtained from MATLAB, VACCALC, and MOLFLOW software, and actual measured data, particularly for a 100 Ah dose. The disparities between model outcomes and observed measurements can be attributed to the following factors. Firstly, MATLAB and VACCALC adopt a 1D model, not accounting for the lateral dimensions of complex vacuum chambers that influence the actual averaged pressure. Secondly, the model's assumption of CO-equivalent residual gas disregards the actual distribution of gas species within the accelerator vacuum system. Thirdly, variations in sensitivity among total pressure gauges of different types introduce variance in vacuum measurements. Lastly, deviations in vacuum vessel cleaning and conditioning times can lead to desorption outcomes differing from the model's assumptions.

The pursuit of an optimal average dynamic pressure of 1×10^{-9} mbar, as targeted in this study, directly enhances the sustained operational efficiency of the accelerator, thereby enabling beam lifetimes spanning 1 to 20 hours.

Acknowledgments

The authors would like to thank Mr. Adel Amro who is the in charge of vacuum lab at SESAME light source for recording experimental data for storage ring.

This article was supported by the Lublin University of Technology (Grant No. FD-20/IS-6/002).

REFERENCES

1. Vignola, G.; Amro, A.; Attal, M.; Makahleh, F.; Shehab, M.M.; Varnasseri, S. SESAME in Jordan. In: Proceedings of the 2005 Particle Accelerator Conference; IEEE, 2005; 586–589.
2. Vignola, G.; Attal, M. SESAME Lattice. Tech. Note O-1 2004.
3. Attal, M.; Huttel, E.; Manukyan, K.; Saleh, I.; Foudeh, D.; Makahleh, F.; Shehab, M.; Jafar, S.; Abid, I.; Ismail, A. Commissioning of SESAME Booster. In: Proceedings of the 7th Int. Particle Accelerator Conf. (IPAC'16), Busan, Korea, May 8-13, 2016; JACOW, Geneva, Switzerland, 2016; 2880–2882.
4. Biasci, J.C.; Bouteille, J.F.; Carmignani, N.; Chavanne, J.; Coulon, D.; Dabin, Y.; Ewald, F.; Farvacque, L.; Goirand, L.; Hahn, M. A Low-Emittance Lattice for the ESRF. Synchrotron Radiat. News 2014, 27, 8–12.
5. Foerster, C.L.; Halama, H.; Lanni, C. Photon-stimulated desorption yields from stainless steel and copper-plated beam tubes with various pretreatments. J. Vac. Sci. Technol. A Vacuum, Surfaces, Film. 1990, 8, 2856–2859.
6. Herbeaux, C.; Marin, P.; Baglin, V.; Gröbner, O. Photon stimulated desorption of an unbaked stainless steel chamber by 3.75 KeV critical energy photons. J. Vac. Sci. Technol. A Vacuum, Surfaces, Film. 1999, 17, 635–643.
7. Margaritondo, G. Elements of Synchrotron Light: For Biology, Chemistry, and Medical Research; Oxford University Press, 2002.
8. Henstridge, M.; Pfeiffer, C.; Wang, D.; Boltasseva, A.; Shalaev, V.M.; Grbic, A.; Merlin, R. Synchrotron radiation from an accelerating light pulse. Science, 2018, 362, 439–442.
9. Martelli, S.; Perilli, E. Time-elapsed synchrotron-light microstructural imaging of femoral neck fracture. J. Mech. Behav. Biomed. Mater. 2018, 84, 265–272.
10. Budiman, A.S.; Illya, G.; Anbazhagan, S.; Tippabhotla, S.K.; Song, W.J.; Sahay, R.; Tay, A.A.O. Enabling lightweight polycarbonate-polycarbonate (PC-PC) photovoltaics module technology–enhancing integration of silicon solar cells into aesthetic design for greener building and urban structures. Sol. Energy 2022, 235, 129–139.
11. Beal, R.E.; Hagström, N.Z.; Barrier, J.; Gold-Parker, A.; Prasanna, R.; Bush, K.A.; Passarello, D.; Schelhas, L.T.; Brüning, K.; Tassone, C.J. Structural origins of light-induced phase segregation in organic-inorganic halide perovskite photovoltaic materials. Matter 2020, 2, 207–219.
12. Thomas, S.E.; Collins, P.; James, R.H.; Mendes, V.; Charoensutthivarakul, S.; Radoux, C.; Abell, C.; Coyne, A.G.; Floto, R.A.; Von Delft, F. Structure-guided fragment-based drug discovery at the synchrotron: screening binding sites and correlations with hotspot mapping. Philos. Trans. R. Soc. A 2019, 377, 20180422.
13. Chan, K.L.A.; Lekkas, I.; Frogley, M.D.; Cinque, G.; Altharawi, A.; Bello, G.; Dailey, L.A. Synchrotron photothermal infrared nanospectroscopy of

drug-induced phospholipidosis in macrophages. Anal. Chem. 2020, 92, 8097–8107.

14. Souza, B.E.; Donà, L.; Titov, K.; Bruzzese, P.; Zeng, Z.; Zhang, Y.; Babal, A.S.; Möslein, A.F.; Frogley, M.D.; Wolna, M. Elucidating the drug release from metal–organic framework nanocomposites via in situ synchrotron microspectroscopy and theoretical modeling. ACS Appl. Mater. Interfaces 2020, 12, 5147–5156.
15. Alhusban, A.A.; Albustanji, S.; Hamadneh, L.A.; Shallan, A.I. High performance liquid chromatography–tandem mass spectrometry method for correlating the metabolic changes of lactate, pyruvate and l-glutamine with induced tamoxifen resistant MCF-7 cell line potential molecular changes. Molecules 2021, 26, 4824.
16. Einfeld, D.; Hasnain, S.S.; Sayers, Z.; Schopper, H.; Winick, H. SESAME, a third generation synchrotron light source for the middle east region. Radiat. Phys. Chem. 2004, 71, 693–700.
17. Makahleh, F.; Amro, A. Storage ring vacuum system performance evaluation.
18. Sullivan, M.K. A method for calculating pressure profiles in vacuum pipes. PEP-II AP Note 1994, 6, 94.
19. Huttel, E.; Einfeld, D. The vacuum system for the synchrotron radiation source ANKA. In: Proceedings of the Particle Accelerator Conference (Cat. No. 97CH36167); IEEE, 1997; 3, 3613–3615.
20. Kersevan, R.; Pons, J.-L. Introduction to MOLFLOW+: New graphical processing unit-based monte carlo code for simulating molecular flows and for calculating angular coefficients in the compute unified device architecture environment. J. Vac. Sci. Technol. A, 2009, 27, 1017–1023.
21. Al-Najdawi, M.; Huttel, E.; Makahleh, F.; Shehab, M.; Al-Mohammad, H. Vacuum system of SESAME storage ring. In: Proceedings of the 9th Edition of the Mechanical Engineering Design of Synchrotron Radiation Equipment and Instrumentation Conference (MEDSI'16), Barcelona, Spain, 11-16 September 2016; JACOW Publishing, Geneva, Switzerland, 2017; 71–73.
22. Ma, Q.; Xu, Z.; Wang, R.; Poredoš, P. Distributed vacuum membrane distillation driven by direct-solar heating at ultra-low temperature. Energy 2022, 239, 121891.
23. O'Hanion, J.F. User Guide to Vacuum Technology. 2nd Ed.; John Wiley and sons Inc., USA, 1989.
24. Solyman, A.A.A.; Qudaimat, A.; Tamizi, K. Simple mathematical and Simulink model of stepper motor. Energies 2022, 15, 6159. https://doi.org/10.3390/en15176159
25. Makahleh, F.; Badran, A.; Attar, H.; Amer, A.; Al-Almaaitah, A. Modeling and simulation of a two stage adsorption chiller with heat recovery, Part 2. J. Appl. Sci. 2022, 12, 5156.
26. Makahleh, F.M.; Badran, A.A.; Attar, H.; Amer, A.; Al-Maaitah, A.A. Modeling and simulation of a two-stage air cooled adsorption chiller with heat recovery. Part I: Physical and mathematical performance model. Appl. Sci. 2022, 12, 6542. https://doi.org/10.3390/app12136542